J Radioanal Nucl Chem (2017) 311:2029–2037
DOI 10.1007/s10967-016-5128-3

Preparation of hollow SiO_2 microspheres functionalized with amidoxime groups for highly efficient adsorption of U(VI) from aqueous solution

Ying Dai[1] · Jieyun Jin[1,2] · Limin Zhou[1,3] · Tianqi Li[1] · Zhao Li[1] · Zhirong Liu[1,2] · Guolin Huang[1] · Adesoji A. Adesina[3]

Received: 5 November 2016 / Published online: 17 December 2016

Abstract The amidoxime-functionalized hollow SiO_2 microspheres (HSA) were prepared for highly efficient U(VI) adsorption. Results showed that amidoxime modification could improve both sorption capacity and sorption selectivity for U(VI), however, excess functionalization might block the mesopores and thus restricting U(VI) sorption. The maximum U(VI) sorption capacity was 109.6 mg/g for HSA15 at 298 K and pH 5.0. The U(VI) sorption isotherms could be described by Langmuir model; whereas the sorption kinetics fitted well with the pseudo-second-order equation, indicating of monolayer chemisorption mechanism. The HSA sorbents could be efficiently regenerated by 0.6 M HNO_3 and reused for several sorption–desorption cycles.

Keywords SiO_2 microspheres · Functionalization · Amidoxime · U(VI) sorption

Electronic supplementary material The online version of this article (doi:10.1007/s10967-016-5128-3) contains supplementary material, which is available to authorized users.

✉ Jieyun Jin
jingjieyun111@sohu.com

✉ Limin Zhou
minglzhecit@sohu.com

[1] State Key Laboratory for Nuclear Resources and Environment, East China University of Technology, 418 Guanglan Road, Nanchang 330013, People's Republic of China

[2] Radioactive Geology and Exploration Technology Laboratory, East China University of Technology, 418 Guanglan Road, Nanchang 330013, People's Republic of China

[3] School of Chemical Sciences and Engineering, University of New South Wales, Sydney 2035, Australia

Introduction

Uranium is an important fuel for nuclear reactors but the uranium resources are in shortage due to rapid increase of nuclear energy. On the other hand, uranium-containing wastewater arised from uranium processing is very dangerous and need to be treated because of its toxicity and radioactivity [1]. Different methods have been developed for the separation of uranium, among them sorption is mostly adopted since it has the advantages of easy operation, low cost, and wide adaptability [2]. Many kinds of materials such as ion-exchange resins, alumina, activated carbon, and polymers have been investigated for uranium sorption [3–7]. However, most of these materials suffered from weak stability, low ion selectivity, or bad cost effectiveness, thus restricting their practical application.

The mesoporous SiO_2 materials have excellent mechanical strength and radiation stability, as well as some unique features such as large surface area, tunable pore size, and facile modification [8, 9], and thus become ideal sorbents for the separation of radionuclides. Compared to conventional silica-based materials, the hollow mesoporous silica (HMS) microspheres have more suitable apparent density for better dispersion in solution; Moreover, HMS have much less inner-particle diffusion resistance, thus enhancing kinetic rate for radionuclide separation. The formation of ordered-mesopores in HSM provides a quick access of the sorption centers for radionuclides.

The sorption capacity or the sorption selectivity of HMS for radionuclides could be improved by grafting different functional groups such as phosphoric acid [9], amino [10], thiol [11], thiadiazole [12], and amidoxime [13, 14]. These groups have high affinity towards various radionuclide ions (Lewis acid) since they contain electronegative donor atoms (Lewis base) such as N, P, O, and S, etc. For uranly

ions chelation, amidoxime has been shown to be an excellent amphoteric functional group since it contains both acidic oxime and basic amino groups [13–15]. Different amidoxime-functionalized materials have been investigated for U(VI) sorption, and the results have shown that amidoxime functionalization could improve sorption capacity or selectivity for U(VI) [14, 15].

In this work, the hollow SiO_2 microspheres functionalized with amidoxime groups (HSA) were synthesized and their sorption properties towards U(VI) were investigated. The amount of functional agents was varied and optimized for the evaluation of this factor on U(VI) sorption. It was interesting to find that the incorporation of excess amount of tri-functional silanes might destroy or block the ordered-mesoporous structures, and this may result in the decrease of sorption capacity for U(VI).

Experimental

Reagents and materials

Polystyrene (PS) microspheres (about 400 μm diameter, used as hard-template for synthesis) were obtained by sieving of PS resins (Yanzhou Huitong Resins Co. Ltd., China). Cyanopropyltriethoxysilane (CPTS) and P123 were purchased from Gelest in Morrisville, PA (USA). Tetraethyl orthosilicate (TEOS), tetrahydrofuran (THF) and other chemicals with the analytical purity were purchased from Sinopharm Chemical Reagent Co. Ltd.

Preparation of amidoxime-functionalized hollow SiO_2 microspheres (HSA)

The preparation of hollow SiO_2 microspheres (HS) using PS as a hard-template and P123 as a co-template was similar to the procedure described in the Ref. [16]. The difference is to use P123 instead of CTAB as a co-template since it allows for the synthesis of mesoporous silica-based materials with relatively thick pore walls, which enhances the mechanical stability of the resulting mesoporous structures [9]. The functionalized HS was obtained by the initial condensation reaction of functional organic silanes (CPTS) with the hydroxyl groups of SiO_2 (HS–CPTS). After that the HS–CPTS (1.0 g) were reacted with hydroxylamine (1.5 g) in the presence of sodium carbonate (1.5 g) in 100 mL water–ethanol (5: 1.6 v/v) solution at 70 °C for 12 h to afford the corresponding amidoxime derivatives (HSA). The mole ratio of TEOS and CPTS (TEOS/CPTS) was controlled to be 10:0 (HS, without CPTS); 10: 1.0 (HSA10) 10: 1.5 (HSA15), and 10: 2.0 (HSA20), respectively. The final products were separated, washed throughly and dried at 60 °C under vacuum. The typical synthesis procedure of HSA15 is shown in Scheme 1.

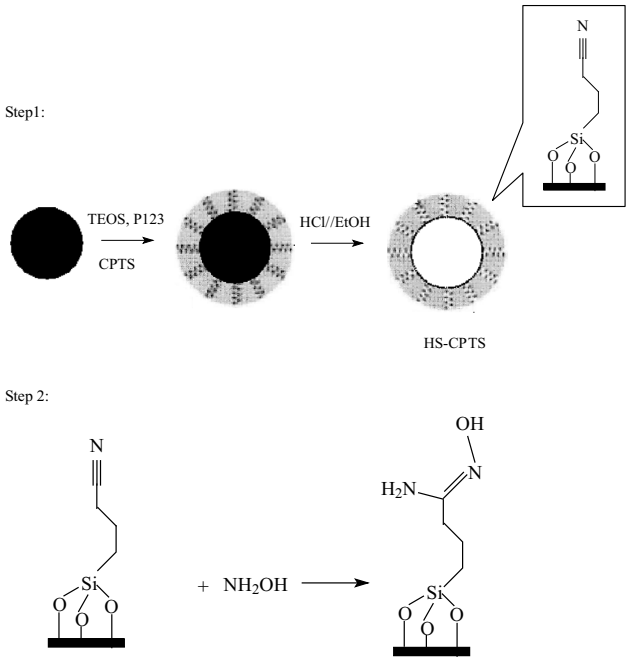

Scheme 1 The synthesis procedure of HSA15

Characterization

The SEM image was observed by a Leica Cambridge S360 scanning electron microscope. Small-angle X-ray diffraction patterns (SAXRD) were taken on an X′ Pert-Pro MPD X-ray diffractometer. FT-IR spectra were measured on a Nicolet, Magna-550 spectrometer. The nitrogen sorption–desorption isotherms were obtained by using a ASAP 2010 volumetric analyzer. Thermal gravimetric analysis of the sorbents was conducted on Shimadzu TGA-50H with heating rate of 10 °C/min in the nitrogen flow. The elemental analysis of the samples was performed in the Laboratory of Chinese Academy of Science (Beijing).

Sorption/desorption experiments

50 mg of sorbents were mixed with 100 mL of U (VI) solution for sorption at 25 °C and the stirring speed of 150 rpm. The initial pH of the solution was controlled by adding small amount of 0.5 M NaOH and/or $HClO_4$ solutions. After sorption for 5 h, samples (about 1 mL) were taken and the sorbents were separated by centrifugalization. The U(VI) concentration in the supernatant was analyzed by Arsenazo-III spectrophotometric method (Shimadzu UV-1601 spectrophotometer).

The selective sorption of U(VI) was conducted in simulated wastewater containing U(VI) and co-existing cations

(Ni^{2+}, Cu^{2+}, Co^{2+}, Sm^{3+}, Ce^{3+}, and Eu^{3+}). The initial concentration of each metal is 5 mg/L. The final metal concentration in the mixture was analyzed by using a ARL-340 Inductively Coupled Plasma (ICP-AES Fison Instruments).

The amount of U(VI) adsorbed (q_e), the distribution coefficient (K_d), and the selectivity coefficient of U(VI) ($S_{U/M}$) were calculated as follows:

$$q_e = (C_0 - C_e) \times \frac{V}{m}, \quad (1)$$

$$K_d = \frac{C_0 - C_e}{C_e} \times \frac{V}{m}, \quad (2)$$

$$S_{U/M} = \frac{K_{d,U}}{K_{d,M}}, \quad (3)$$

where C_0 and C_e are the initial and equilibrium U(VI) concentrations, respectively (mg/L); q_e is the sorption capacity (mg/g); V is the volume of U(VI) solution (L); and m is the mass of the sorbents (g).

Results and discussion

Characterization

Figure 1a shows the surface morphology of amidoxime-functionalized hollow silica microspheres (HSA15). The surface of HSA15 is un-smooth due to the incorporation of organic silanes. The HSA15 has a hollow structure, which can be seen from the hole in the surface of the microsphere. The diameter of HSA15 is about 500–600 nm, and the shell-thickness is around 80–100 nm.

The FTIR spectra of HS–CPTS and HSA15 are shown in Fig. 1b, which confirm the existence of the funtional groups. The peaks at 462 cm^{-1} (O–Si–O bending vibration) and 1075 cm^{-1} (Si–O–Si and Si–O–H stretching vibration [9]) appear at the spectra of both HS–CPTS and HSA15. The band for the C≡N stretching vibration could be identified at 2272 cm^{-1}, arising from the co-condensation of TEOS with CPTS. After amidoxime functionalization, the C≡N absorption band became weaken, whereas two other new peaks appeared at 1605 cm^{-1} (C=N stretching vibration) and 942 cm^{-1} (N–O stretching vibration [13]), respectively; indicating of the successful amidoxime functionalization for the silica microspheres.

The diffraction peak at $2\theta = 1.2°$ for HSA15 in SAXRD (Fig. S1a) confirms the presence of mesoporous structure. Meanwhile, the N_2 sorption–desorption isotherm of HSA15 (Fig. S1b) shows a type-IV curve, which further confirms the mesoporous framework of HSA15. The pore size distributions (PSD) (Fig. S1c) shows that HSA15 has a narrow peak centered at 4.5 nm, indicating of the mesoporous

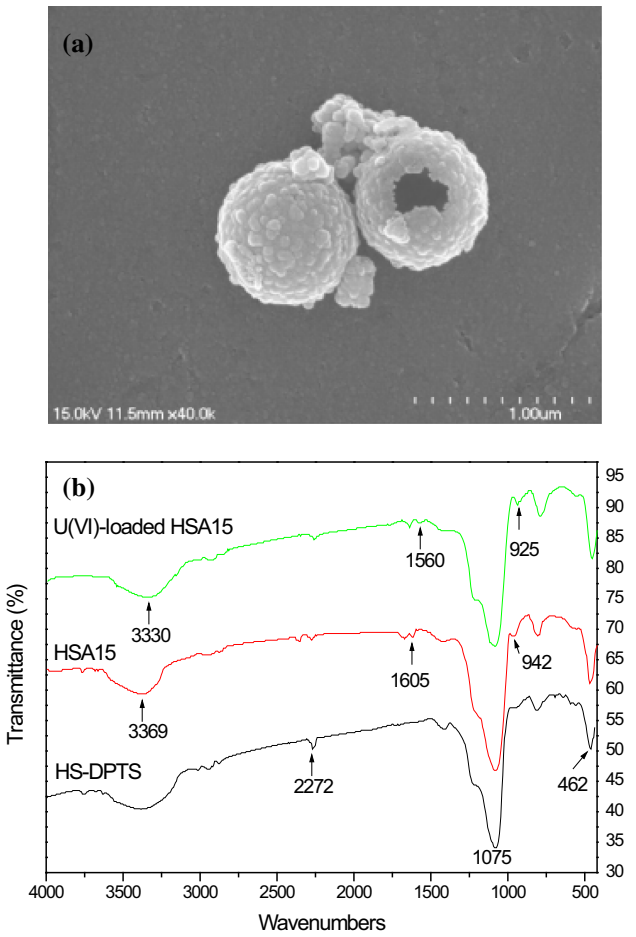

Fig. 1 The SEM images of HSA15 (**a**) and FT-IR spectra of HS–CPTS, HSA15, and U(VI)-loaded HSA15 (**b**)

structure. From the thermogravimetric (TG) and derivative thermogravimetric (DTG) curves of HSA15 (Fig. S1d), the weight loss for the two decomposition stages (corresponding to the two DTG peaks at 258–413 and 494–620 °C) due to the decomposition of organic moieties is about 10.8%, thus the amount of amidoxime groups (the molecular mass of organic moieties is 101 u) for HSA15 is calculated to be 1.06 mmol/g.

Effect of pH and ionic strength

The effect of pH on U(VI) sorption on HSA15 is shown in Fig. 2. It can be seen that U(VI) sorption efficiency increases with increasing pH at lower pH range (pH < 5.0), but after reaching the maximum value, it decreases at higher pH values (pH > 6.0). This can be explained by both the U(VI) species distribution and the complexation between U(VI) and amidoxime groups.

The distribution of U(VI) species with pH (Fig. S2) indicates that uranyl ions are the main species at lower pH, whereas other species such as $UO_2(OH)_3^-$ and

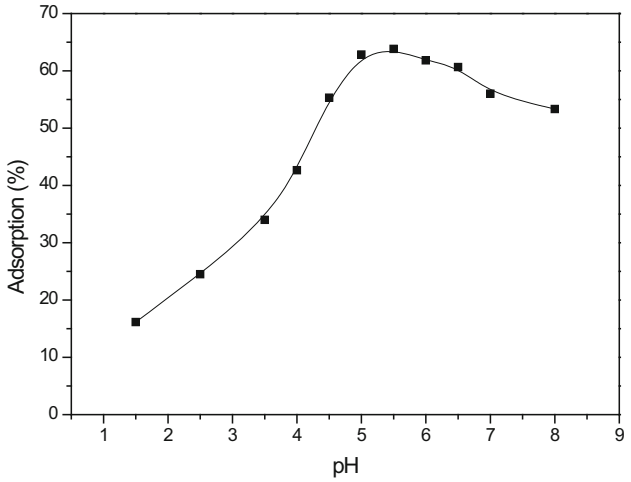

Fig. 2 Effect of initial pH on the sorption of U(VI) ions onto HSA15 ($C0 = 30$ mg/L; $T = 298$ K; sorbent dosage, SD = 0.5 g/L)

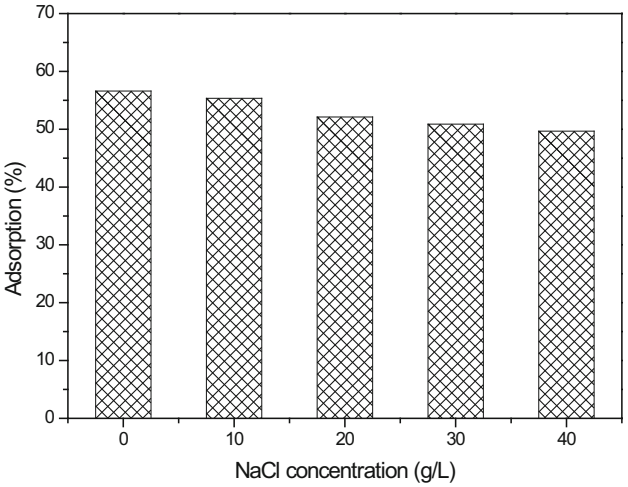

Fig. 3 Effects of NaCl concentrations on the sorption of U(VI) ions onto HSA15

$(UO_2)_3(OH)_7^-$ appear at higher pH. The oxime oxygen of the amidoxime group can undergo metal-assisted deprotonation [15]:

$$R{-}C(NH_2)N{-}OH \rightleftharpoons R{-}C(NH_2)N{-}O^- + H^+, \quad (4)$$

$$2R{-}C(NH_2)N{-}O^-UO_2^{2+} \rightleftharpoons UO_2(R{-}C(NH_2)N{-}O^-)_2. \quad (5)$$

As pH increases, more H^+ ions released from the deprotonation reaction (Eq. 4) are neutralized, so the competitive sorption from H^+ ions decreased and the electrostatic repulsion between positive uranyl ions and HSA15 weakened. This is favorable for uranyl ions sorption and thus U(VI) sorpiton efficiency increases. However, at higher pH values (pH > 6.0), more non-complexible species (such as $UO_2(OH)_3^-$ and $(UO_2)_3(OH)_7^-$) formed and the electrostatic repulsion between these anions and the negatively charged surface of HSA15 increased, thus U(VI) sorption efficiency decreased.

To determine the influence of the ionic strength on U(VI) sorption, NaCl with different concentration was added to the U(VI) solution. Figure 3 shows that the U(VI) removal efficiency slightly decreased (about 10%) when the NaCl concentration reached 40 g/L, suggesting that the ionic strength has a weak influence on U(VI) sorption. These results indicate that the removal of U(VI) is dominated by inner-sphere surface chelation [9]. The weak effect of ion strength makes it possible to use HSA15 sorbent in the treatment of high salinity wastewater or even in the extraction of U(VI) form salt lake brines.

Sorption kinetics

Figure 4 shows the sorption kinetic curves of U(VI) by HSA15. Two sorption stages are found for the kinetic

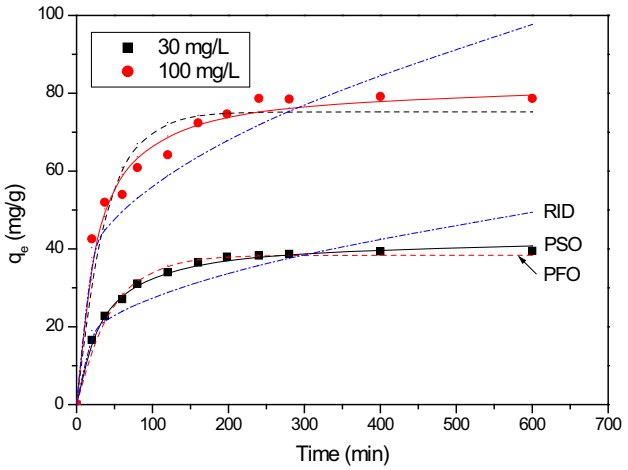

Fig. 4 Effect of contact time on the sorption of U(VI) ions onto HSA15 at different initial concentrations (pH 5.0; $T = 298$ K; sorbent dosage, SD = 0.5 g/L)

curves: the initial rapid sorption followed by the slow sorption until gradually reaching equilibrium at 5 h. On the first stage, the greater U(VI) concentration gradient and more available spare active sites are contributed to the rapid U(VI) sorption; whereas on the second stage, both U(VI) concentration gradient and spare active sites decrease, resulting in the decrease of kinetic rate. Compared to other silica-based sorbents (which usually need long time to achieve equilibrium) [8, 9], HSA15 had fast sorption kinetic rate for U(VI) due to the well-developed mesoporous structures and the strong chelation between U(VI) and amidoxime groups. The initial U(VI) concentration also has some effects on the sorption kinetics: apparently longer equilibrium time is needed at higher initial U(VI) concentration.

The U(VI) sorption by the resins usually contains multisteps: bulk diffusion, external film diffusion, intraparticle diffusion, and chemisorption on the active sites [17, 18]. To determine the rate-controlling step, the sorption kinetic data were fitted by different kinetic models, including the pseudo first-order (PFO) (Eq. 6), the pseudo second-order (PSO) (Eq. 7), and the resistance to intraparticle diffusion (RID) models (Eq. 8) [17]:

$$q_t = q_e(1 - e^{-k_1 t}), \tag{6}$$

$$q_t = \frac{q_e^2 k_2 t}{1 + q_e k_2 t}, \tag{7}$$

$$q_t = k_{int} t^{1/2} + C, \tag{8}$$

where q_e (mg/g) is equilibrium sorption capacity, q_t (mg/g) is the sorption capacity at time t (min); k_1 (min^{-1}), k_2 (g mg^{-1} min^{-1}), and k_{int} (mg/g min$^{-0.5}$) are the rate constants for the PFO, PSO, and RID, respectively.

The kinetic parameters for the above kinetic models are summarized in Table 1. The fitting curves are also shown in Fig. 4. Obviously PSO has the highest R^2 values ($R^2 > 0.99$) among the three kinetic models. Moreover, the sorption capacities obtained by PSO model ($q_{e,\ cal}$) is also close to the experimental values ($q_{e,\ exp}$). These results indicate that PSO model is suitable for fitting the kinetic data for U(VI) sorption onto HSA15, implying that chemisorption (or surface chelation between amidoxime and U(VI)) is the rate-controlling step. The RID model showed a large deviation with the kinetic data, indicating that the intraparticle diffusion have a negligible effect [18]. The effect of both bulk diffusion and external film diffusion is small due to the rapid stirring during U(VI) sorption.

Sorption isotherms and thermodynamics

The U(VI) sorption isotherms are shown in Fig. 5, which could provide useful information for describing the equilibrium distribution of U(VI) between the liquid and the solid phases. As shown in Fig. 5a, temperature shows a positive effect on U(VI) sorption, indicating of the endothermic nature of the sorption process. To further clarify the U(VI) sorption mechanism, the sorption isotherms were fitted by Langmuir Eq. (9) and Freundlich Eq. (10) models [17, 19]:

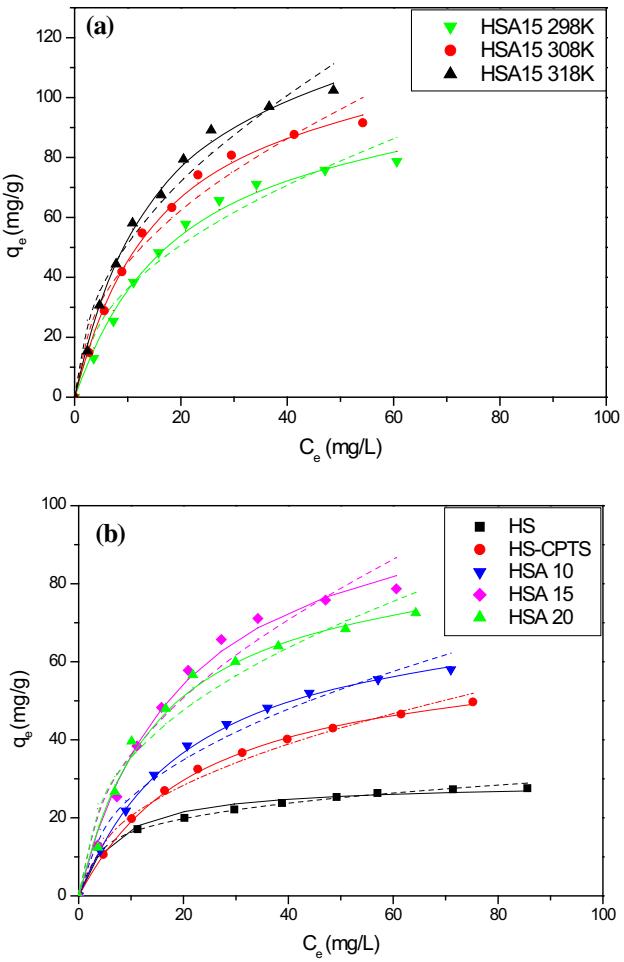

Fig. 5 Isotherms of U(VI) sorption onto HSA15 at different temperature (**a**); and U(VI) sorption onto the different silica-based sorbents at 298 K (**b**). (the *solid lines* represent Langmuir model whereas the *dash lines* represent Freundlich model; $C_0 = 10$–100 mg/L; $T = 298$–308 K; pH 5.0; $t = 160$ min; SD = 0.5 g/L)

$$q_e = \frac{K_L q_m C_e}{1 + K_L C_e}, \tag{9}$$

$$q_e = k_F C_e^{1/n}, \tag{10}$$

where C_e is U(VI) equilibrium concentration (mg/L), q_m is the maximum U(VI) sorption capacity (mg/g), K_L (L/mg) and K_F are constants for the Langmuir and Freundlich models, respectively; n is a constant related to sorption intensity.

Table 1 Kinetic parameters of the sorption of U(VI) onto HSA15 at different concentrations

Conc.		PFO		R^2	PSO		R^2	RID		R^2
(mg/L)	$q_{e,\ exp}$ (mg/g)	$k_1 \times 10^2$ (min^{-1})	$q_{e,\ cal}$ (mg/g)		$k_2 \times 10^4$ (g/mg/min)	$q_{e,\ cal}$ (mg/g)		k_i (mg/g min$^{-0.5}$)	X	
30	39.5	2.26	38.4	0.973	7.33	42.9	0.997	1.52	12.3	0.759
100	78.7	2.78	75.2	0.945	5.07	82.7	0.982	2.86	27.5	0.742

The isotherm model parameters are shown in Table 2. Compared to Freundlich model, Langmuir model had higher R^2 values ($R^2 > 0.99$) and fitted better with the isotherms (Fig. 5), suggesting the monolayer sorption (or chemisorption) mechanism for U(VI) sorption. Moreover, both q_{max} and k_L values increased with temperature for HSA15. Higher temperature is favorable for U(VI) sorption at higher energy active sites, thus enhancing U(VI) sorption [19, 20].

The thermodynamics parameters were calculated by the van't Hoff equation [18]:

$$\ln K_L = \frac{-\Delta H^0}{RT} + \frac{\Delta S^0}{R} \quad (11)$$

$$\Delta G^0 = \Delta H^0 - T\Delta S^0, \quad (12)$$

where ΔG^0 is Gibbs free energy change (J/mol), ΔH^0 is enthalpy change (J/mol), ΔS^0 is entropy change (J/(mol K)).

The thermodynamics parameters are given in Table 3. The fitting van't Hoff equation is: $\ln K_L = -1082.3/T + 13.022$ ($R^2 = 0.9775$). The positive ΔH^0 and the negative ΔG^0 values indicate that U(VI) sorption on HSA15 is endothermic and spontaneous. Meanwhile, ΔG^0 values become more negative as temperature increases, indicating that U(VI) sorption is enhanced at higher temperatures [18].

As shown in Table 2 and Fig. 5b, the U(VI) sorption capacity (q_m) obtained for HSA15 is highest among the five silica-based sorbents. This sorbent has relatively uniform mesopores, which are easily accessible for uranium species in solution. The sorption capacities of HSA are much higher than those of HS and HS–CPTS due to functionalization of amidoxime groups. The q_m of HSA15 is almost 1.5 times of that of HSA10, which is not surprising since the amidoxime content in HSA15 is about 1.5 times too (Table 4). The BET surface area for HSA15 is about 7% lower than that of HSA10, probably due to incorporation of more functional silanes. In comparison with HSA15, HSA20 contains even more amidoxime groups, and thus it could be expected that HSA20 had higher U(VI) sorption capacity. In contrast with this, Table 2 shows that the q_m for HSA20 is almost 20% smaller than that for HSA15, probably due to the introduction of excess amount of functional agents (CPTS). In this case the well-ordered mesopores may be blocked, thus some active sites are inaccessible to the relatively large U(VI) species. This situation may become even more serious after the binding of initial U(VI) species, which block the access of other U(VI) species. As shown in Table 4, the decreased BET surface area (S_{BET}), pore volume (V_s), as well as (d_m) for HSA20 (compared to HSA15) also partly supports this hypothesis. These results indicated that amidoxime modification could improve sorption capacity for U(VI),

Table 2 Isotherm model parameters for U(VI) sorption by different silica-based sorbents

Sorbents	Temp. (K)	Langmuir		R^2	Freundlich		R^2
		q_m (mg/g)	$k_L \times 10^2$ (L/mg)		k_F (mg/g) (L/mg)$^{1/n}$	n	
HS	298	29.1	14.33	0.998	9.25	3.91	0.979
HS–CPTS	298	51.8	4.39	0.992	7.32	2.20	0.973
HSA10	298	76.3	4.73	0.999	9.01	2.21	0.976
HSA20	298	89.9	6.72	0.990	13.66	2.39	0.952
HSA15	298	109.6	4.91	0.992	12.08	2.08	0.956
	308	123.4	5.95	0.996	15.29	2.13	0.967
	318	139.8	6.16	0.997	16.79	2.06	0.970

Table 3 Thermodynamic parameters of U(VI) by HSA15

Temp. (K)	ΔG^0 (kJ/mol)	ΔH^0 (kJ/mol)	ΔS^0 (J/mol K)	$T\Delta S^0$ (kJ/mol)	R^2
298	−23.26	8.998	108.26	32.26	0.9775
308	−24.35			33.35	
318	−25.43			34.43	

Table 4 The sturcuture characteristics for different silica-based sorbents

Samples	Active sites (mmol/g)	TEOS/CPTS (mole ratio)	S_{BET} (m^2/g)	V_s (cm^3/g)	d_m (nm)
HS	–	10:0	382	0.98	5.8
HSA10	0.67	10:1.0	334	0.78	4.7
HSA15	1.06	10:1.5	312	0.65	4.4
HSA20	1.25	10:2.0	281	0.38	3.9

however, excess functionalization might block the mesopores and thus restricting U(VI) sorption.

Sorption mechanism

It was reported that the amidoxime groups could act as efficient chelation groups for uranyl ions [16, 21]. Figure 6 shows the two possible structures for uranyl ions chelating with amidoxime. In Fig. 6a, the lone pairs of electrons on two oxygen atoms and two nitrogen atoms are donated to the positive uranyl ions center to form a five-membered chelating structure (including U(VI)). Different from Fig. 6a, b shows that four oxime oxygen atoms are incorporated with uranyl ions to form a five-membered chelating structure. From the results obtained in this work, the U(VI) sorption capacity for HAS15 is 109.6 mg/g (or 0.46 mmol/g), whereas the amidoxime group content is 1.06 mmol/g; which means that one uranyl ion is approximately incorporated with two amidoxime groups (U(VI)/amidoxime mole ratio is close to 1/2). Thus the structure shown in Fig. 6a is more likely to be the chelating structure for U(VI) sorption on HAS15.

To further clarify the sorption mechanism, the FTIR spectrum for the U(VI)-loaded HAS15 was obtained (Fig. 1b). After uranium sorption, the peak at the wave number of 3369 cm^{-1}, corresponding to the stretching vibration of the –OH and $–NH_2$ groups, decreases to 3330 cm^{-1}. Meanwhile, the band of C=N stretching vibration at 1605 cm^{-1} for HAS15 shifts to 1560 cm^{-1} after uranium sorption. These results indicate that U(VI) sorption affects the chemical bonds of the nitrogen atoms in the amidoxime groups. Moreover, there is a new peak at 925 cm^{-1} on the FTIR spectrum for U(VI)-loaded HAS15, which can be attributed to the stretching vibration of O=U=O [15]. The element analysis results indicated that the element compositions for HAS15 before U(VI) sorption are: C 5.1%, H 1.0%, N 2.9%, and Si 26.6%; while for the U(VI)-loaded HAS15, the element compositions are: C 4.7%, H 0.8%, N 2.5%, Si 24.8%, and U 6.9%, respectively. The decrease of C, H, N, and Si contents for HAS15 after U(VI) sorption is due to U(VI) loading onto the sorbents.

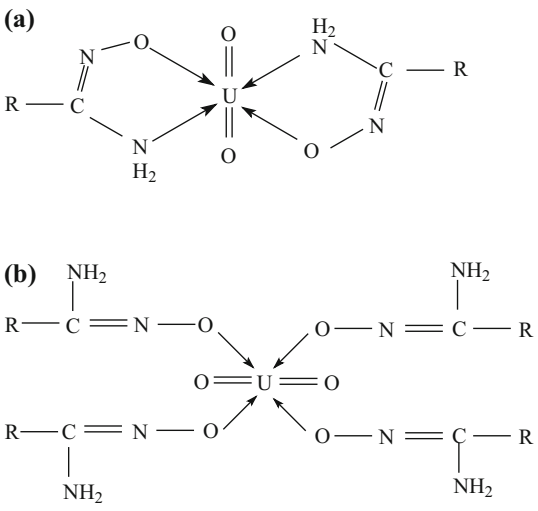

Fig. 6 The possible structures for the chelation of amidoxime groups with uranyl ions

Selectivity studies

The selectivity coefficients ($S_{U/M}$) of U(VI) with respect to other cations (Ni^{2+}, Cu^{2+}, Co^{2+}, Sm^{3+}, Ce^{3+}, and Eu^{3}) are shown in Fig. S3. The $S_{U/M}$ values of HSA for all co-existing cations are remarkably improved compared to those of unmodified hollow silica microspheres (HS). Except for Sm^{3+}, the $S_{U/M}$ values of HSA for all other cations increased by more than 3 times compared to those of HS. These results indicate that amidoxime groups are very effective for the selective chelation of U(VI), and HSA has an excellent selectivity towards uranyl ions in the solution containing of U(VI) and other co-existing cations.

Comparison with other adsorbents

Table 5 shows the sorption capacities of different sorbents for U(VI) sorption. Since the sorption conditions (such as sorbent dosage, contact time, solution composition, and pH values) are different in the experiments, it is hard to make a direct comparison. However, this comparison could still provide some useful information for the evaluation of the sorbents. As shown in Table 5, HSA15 has a relatively high U(VI) sorption capacity, although its q_m value is lower than those reported in some references [8, 22]. However, this sorbent has fast uptake kinetic as well as excellent selectivity for U(VI) sorption as discussed above. These results indicated that the HSA15 could be a promising adsorbent for the efficient separation of U(VI) from aqueous solution.

Desorption and regeneration of the sorbents

The U(VI) desorption experiments were conducted by shaking 0.15 g of the U(VI)-loaded HSA15 (U(VI) initial concentration 100 mg/L) with 30 mL of desorbing agents. When 0.6 M HCl, 0.6 M HNO_3, 0.6 M Na_2CO_3, or 0.6 M $NaHCO_3$ are used, the desorption efficiency was determined to be 82, 96, 74, and 67%, respectively. Obviously 0.6 M HNO_3 was the most effective desorption agent. Moreover, further increase in the HNO_3 concentration did not show a positive effect for U(VI) desorption. Thus the sorption–desorption cycles were conducted for five times using 0.6 M HNO_3 as the desorption agent. The results

Table 5 Reported sorption capacities of U(VI) by different adsorbents

sorbents	Sorption conditions	q_{max} (mg/g)	Refs.
Phosphonate-modified mesoporous silica (NP10)	$T = 298$ K, pH 6.9	303.0	[22]
Salicylaldehyde-modified magnetic silica	$T = 298$ K, pH 7.0	49.0	[23]
Quercetin-modified magnetic silica	$T = 298$ K, pH 3.7	12.3	[24]
Amine-modified silica gel	$T = 302$ K, pH 4.0	21.4	[25]
Functionalized polymer-coated silica	$T = 298$ K, pH 4.5	5.2	[26]
Organo-functionalized mesoporous silica	$T = 298$ K, pH 8.0	185.2	[8]
HSA10	$T = 298$ K, pH 5.0	76.3	This work
HSA15		109.6	
HSA20		89.9	

showed that the loss of U(VI) sorption capacity (q_{exp}) sorption capacity was less than 12%: q_{exp} decreased from 78.7 mg/g in the first run to 69.2 mg/g in the last run.

Conclusions

The amidoxime-functionalized hollow silica microspheres were synthesized, characterized, and investigated for U(VI) sorption from aqueous solution. It was found that U(VI) sorption by HSA15 was strongly influenced by the pH values, but slightly affected by the ion strength, indicating of the inner-sphere chelation mechanism. The maximum U(VI) sorption capacity (q_m) for HSA15 is 109.6 mg/g (at pH 5.0 and 298 K). The relatively high U(VI) sorption capacity of HSA15 can be attributed to the strong chelation of U(VI) with amidoxime as well as the easy accessibility of mesopore channels. Temperature shows a positive effect on U(VI) sorption. The sorption was endothermic and spontaneous, as evidenced by the positive ΔH^0 and the negative ΔG^0 values. In addition, HSA15 can be efficiently regenerated by 0.6 M HNO_3 and reused for U(VI) sorption with only a slight decrease in U(VI) sorption capacity. The relatively high sorption capacities, fast uptake kinetics as well as excellent selectivity indicated that the HSA could be a promising adsorbent for applications in U(VI)-containing wastewater treatment.

Acknowledgements This work was financially supported by the National Natural Science Fund Program (21366001; 21667001), the International Scientific and Technological Cooperation Projects (2015DFR61020), the Key Research and Development Program of Jiangxi Province (20161BBF60059), the Scientific Research Project from Education Department of Jiangxi Province (GJJ17380), and the Scientific and Technological Cooperation Project of Jiangxi Province (20161BBH80046).

References

1. Sprynskyy M, Kovalchuk I, Buszewski B (2010) The separation of uranium ions by natural and modified diatomite from aqueous solution. J Hazard Mater 181:700–707
2. Dolatyari L, Yaftian MR, Rostamnia S (2016) Removal of uranium(VI) ions from aqueous solutions using Schiff base functionalized SBA-15 mesoporous silica materials. J Environ Manag 169:8–17
3. Heshmati H, Torabmostaedi M, Gilani HG, Heydari A (2015) Kinetic, isotherm, and thermodynamic investigations of uranium(VI) adsorption on synthesized ion-exchange chelating resin and prediction with an artificial neural network. Desalin Water Treat 55:1076–1087
4. Sun Y, Yang S, Sheng G, Guo Z, Tan X, Xu J, Wang X (2012) Comparison of U(VI) removal from contaminated groundwater by nanoporous alumina and non-nanoporous alumina. Sep Purif Technol 83:196–203
5. Fazliismail A, Yim MS (2015) Investigation of activated carbon adsorbent electrode for electrosorption-based urnium extraction from seawater. Nucl Eng Technol 47:579–587
6. Mahfouz MG, Galhoum AA, Gomaa NA, Abdel-Rehem SS, Atia AA, Vincent T, Guiba E (2015) Uranium extraction using magnetic nano-based particles of diethylenetriamine-functionalized chitosan: euilibrium and kinetic studies. Chem Eng J 262: 198–209
7. Villalobos-Rodriguez R, Montero-Cabreraa ME, Esparza-Ponce HE, Herrera-Peraza EF, Ballinas-Casarrubias ML (2012) Uranium removal from water using cellulose triacetate membranes added with activated carbon. Appl Radiat Isot 70:872–881
8. Vivero-Escoto JL, Carboni M, Abney CW, Krafft KE, Lin W (2013) Organo-functionalized mesoporous silicas for efficient uranium extraction. Micropor Mesopor Mat 180:22–31
9. Dudarko OA, Gunathilake C, Wickramaratne NP, Sliesarenko VV, Zub YL, Górka J, Dai S, Jaroniec M (2015) Synthesis of mesoporous silica-tethered phosphonic acid sorbents for uranium species from aqueous solutions. Colloid Surf A 482:1–8
10. El-Toni AM, Habila MA, Ibrahim MA, Labis JP, ALOthman ZA (2014) Simple and facile synthesis of amino functionalized hollow core–mesoporous shell silica spheres using anionic surfactant for Pb(II), Cd(II), and Zn(II) adsorption and recovery. Chem Eng J 251:441–451
11. Hakami O, Zhang Y, Banks CJ (2012) Thiol-functionalised mesoporous silica-coated magnetite nanoparticles for high efficiency removal and recovery of Hg from water. Water Res 46:3913–3922
12. Emadi M, Shams E (2010) Immobilization of thiadiazole derivatives on magnetite mesoporous silica shell nanoparticles in application to heavy metal removal from biological samples. AIP Conf Proc 1311:127–134
13. Kim J, Tsouris C, Oyola Y, Janke CJ, Mayes RT, Dai S, Gill G, Kuo L, Wood J, Choe K, Schneider EA, Lindner H (2014) Uptake of uranium from seawater by amidoxime-based polymeric adsorbent: field experiments, modeling, and updated economic assessment. Ind Eng Chem Res 53:6076–6083

14. Lindner H, Schneider E (2015) Review of cost estimates for uranium recovery from seawater. Energy Econ 49:9–22
15. Zhao YG, Li JX, Zhang SW, Shao D (2013) Efficient enrichment of uranium(VI) on amidoximated magnetite/graphene oxide composites. RSC Adv 3:18952–18959
16. Guo W, Wang J, Lee S, Dong F, Park SS, Ha C (2010) A general pH-responsive supramolecular nanovalve based on mesoporous organosilica hollow nanospheres. Chem Eur J 16:8641–8646
17. Kuang SP, Wang ZZ, Liu J, Wu ZC (2013) Preparation of triethylene-tetramine grafted magnetic chitosan for adsorption of Pb(II) ion from aqueous solutions. J Hazard Mater 260:210–219
18. Rahmati A, Ghaemi A, Samadfam M (2012) Kinetic and thermodynamic studies of uranium(VI) adsorption using Amberlite IRA-910 resin. Ann Nucl Energy 39:42–48
19. Foo KY, Hameed BH (2010) Insights into the modeling of adsorption isotherm systems. Chem Eng J 156:2–10
20. Zhou L, Zou H, Wang Y, Huang Z, Wang Y, Luo T, Liu Z, Adesina AA (2016) Adsorption of uranium(VI) from aqueous solution using magnetic carboxymethyl chitosan nano-particles functionalized with ethylenediamine. J Radioanal Nucl Chem 308:935–946
21. Das S, Pandey AK, Athawale AA, Manchanda VK (2009) Exchanges of uranium(VI) species in amidoxime-funtionalized sorbents. J Phys Chem B 113:6328–6335
22. Yuan LY, Liu YL, Shi WQ, Lv YL, Lan JH, Zhao YL, Chai ZF (2011) High performance of phosphonate-functionalized mesoporous silica for U(VI) sorption from aqueous solution. Dalton Trans 40:7446–7453
23. Rezaei A, Khani H, Masteri-Farahani M, Rofouei MK (2012) A novel extraction and preconcentration of ultra-trace levels of uranium ions in natural water samples using functionalized magnetic-nanoparticles prior to their determination by inductively coupled plasma-optical emission spectrometry. Anal Methods 4:4107–4114
24. Sadeghi S, Azhdari H, Arabi H, Moghaddam AZ (2012) Surface modified magnetic Fe_3O_4 nanoparticles as a selective sorbent for solid phase extraction of uranyl ions from water samples. J Hazard Mater 215:208–216
25. Venkatesan K, Sukumaran V, Antony M, Vasudeva Rao P (2004) Extraction of uranium by amine, amide and benzamide grafted covalently on silica gel. J Radioanal Nucl Chem 260:443–450
26. Bryant DE, Stewart DI, Kee TP, Barton CS (2003) Development of a functionalized polymer-coated silica for the removal of uranium from groundwater. Environ Sci Technol 37:4011–4016